Brain Connectivity

DOI: 10.1089/brain.2016.0450

Brain Connectivity
Test-Retest Reproducibility of the Intrinsic Default Mode Network: Influence of fMRI Slice-Order Acquisition and Head-Motion Correction Methods (doi: 10.1089/brain.2016.0450)
This paper has been peer-reviewed and accepted for publication, but has yet to undergo copyediting and proof correction. The final published version may differ from this proof.

Test-Retest Reproducibility of the Intrinsic Default Mode Network: Influence of fMRI Slice-Order Acquisition and Head-Motion Correction Methods

Rocco Marchitelli* [1,2], Olivier Collignon[1,3], Jorge Jovicich[1]

1 Center for Mind/Brain Sciences (CIMEC), University of Trento, Rovereto, Italy

2 IRCCS, SDN Foundation, Naples, Italy

3 Institute of Research in Psychology (IPSY) and in Neuroscience (IoNS), University of Louvain, Louvain-la-Neuve, Belgium

* Corresponding Author:

Rocco Marchitelli, Ph.D.

IRCCS, SDN Foundation

Via Gianturco, 113, 80143, Naples, Italy

Phone: +39-377-307-2859

E-mail addresses: rocco.marchitelli@aol.com

Keywords

Resting state fMRI, intrinsic functional connectivity, default mode network, motion correction, test-retest reliability, test-retest reproducibility, slice order acquisition, independent component analysis.

Acronyms

DMN = default mode network

FMRI = functional magnetic resonance imaging

TRT reproducibility = test-retest reproducibility

tSNR = temporal signal-to-noise ratio

VOMOCO = volume-based head-motion correction

SLOMOCO = slice-based head-motion correction

PCC/ACC = posterior / anterior cingulate cortex

LPC = latero-parietal cortex

(Group-) ICA = (group) independent component analysis

TR = time resolution

EPI = echo-planar imaging

MPRAGE = magnetization-prepared rapid gradient echo

BOLD = blood oxygenation level dependent

AC-PC = anterior-posterior commissure

ROI(s) = region(s) of interest

GM / WM = gray / white matter

Software acronyms are spelled in the text.

Abstract

Head-motion is a known challenge in resting-state functional magnetic resonance imaging (fMRI) studies for biasing functional connectivity among distinct anatomical regions. These persist even with small motion, limiting comparisons of groups with different head-motion characteristics. This motivates an interest in the optimization of acquisition and correction strategies to minimize motion sensitivity. In this test-retest study of healthy young volunteers (N=23), we investigate the effects of slice-order acquisitions (sequential or interleaved) and head-motion correction methods (volume- or slice-based) on the test-retest (TRT) reproducibility of intrinsic connectivity of the default mode network (DMN). We evaluated the TRT reproducibility of the entire DMN and each main node using the absolute percentage error, intra class correlation coefficient (ICC) and the Jaccard coefficient. Regardless of slice-order acquisition, the slice-based motion correction method systematically estimated larger motion and returned significantly higher temporal signal-to-noise ratio (tSNR). Although consistently extracted across all acquisition and motion correction approaches, DMN connectivity was sensitive to these choices. However, the TRT reproducibility of the whole DMN was stable and showed no sensitivity to the methods tested (absolute reproducibility ~7%, ICC=0.47 and Jaccard=40%). Percentage errors and ICCs were consistent across single nodes but the Jaccard coefficients were not. The posterior cingulate was the most reproducible node (Jaccard=52%) whereas the anterior cingulate was the least reproducible (Jaccard=30%). Our study suggests that the slice-order and motion correction methods evaluated offer comparable sensitivity to detect DMN connectivity changes in a longitudinal study of individuals with low head-motion characteristics but that controlling for the consistency in acquisition and correction protocols is important in cross-sectional studies.

1 Introduction

The Default-Mode Network (DMN) is one of the most studied resting-state functional brain networks. It is made of a set of cortical regions including the posterior and anterior cingulate as well as ventral and dorsal posterior parietal cortices, co-activated when individuals are not involved in overt cognitive task performance (Buckner, 2012; Greicius & Menon, 2004; Greicius et al., 2003; Raichle et al., 2001; Shulman et al., 1997). The DMN has been linked to self-referential processes such as long-term memory retrieval (Andrews-Hanna, 2012), future planning and problem solving (Buckner et al., 2008; Buckner & Carroll, 2007). This network is of particular interest because it can be easily measured from low frequency fluctuations in the blood oxygen level dependent (BOLD) fMRI signal (Biswal et al., 1995), and because it is affected by several neuropsychitaric and neurodegenerative conditions, including autism (Washington et al., 2014), major depression (Mulders et al., 2015), multiple sclerosis (Hawellek et al., 2011) and dementia (Balthazar et al., 2014; Greicius et al., 2004; Hedden et al., 2009; Sheline et al., 2010). This suggests that the DMN itself may serve as a biomarker of neuro-pathophysiological changes in mental illnesses (Binnewijzend et al., 2012; Damoiseaux, 2012).

However, accurate and reproducible characterization of the DMN is challenging because measures of functional connectivity are susceptible to several confounding factors deriving from non-neural fluctuations in the BOLD signal, in particular in-scanner head motion (Murphy et al., 2013). The common presence of micro-movements (< 0.5 mm) exerts global effects throughout the entire brain, spuriously changing the BOLD content across voxels, causing signal distortions or loss (Van Dijk et al., 2012). It has been shown that head-motion artifacts can confound the intrinsic DMN connectivity, enhancing short-range while diminishing long-range connections leading to reduced connectivity in the anterior cingulate cortex (Murphy et al., 2013; Zeng et al., 2014). Furthermore, the inter-subject motion variability hinders comparisons of intrinsic DMN connectivity across groups in cross-sectional designs (Power et al., 2012; Satterthwaite et al., 2012;

Van Dijk et al., 2012; Zeng et al., 2014) whereas individual characteristic motion traits would limit the ultimate sensitivity to neural signals in longitudinal study designs (Zeng et al., 2014; Guo et al., 2012), precluding the development of DMN-based preclinical biomarkers of neurological conditions.

There are two general types of approaches aimed at addressing head-motion correction in MRI studies: one is based on prospective "real-time" measures of head-motion with reorientation of the imaging slices on-the-fly (Godenschweger et al., 2016), and the other is based on retrospective estimation and reorientation of the data after acquisition (Jenkinson et al., 2002). The study of prospective measures is a promising active field of research, but such methods are not yet standardly available and are not further discussed.

Here we focus on retrospective head-motion correction methods, which are more commonly implemented in resting-state fMRI studies (Power et al., 2014). Among these methods, a typical approach consists of a volumetric registration of all brain time series to a reference volume along the entire train of acquisitions (Jenkinson et al., 2002). This procedure yields head translational and rotational parameters that are used to quantify motion, eventually excluding subjects, or only some volumes, compromised by excessive motion (Power et al., 2012). Other methods include the removal of the estimated motion parameters via multiple linear regressions (Satterthwaite et al., 2013) or exploit data-driven methods such as independent component analysis (ICA) to detect and remove motion signals (Pruim et al., 2014; Schöpf et al., 2010, 2011; Griffanti et al., 2014). Although widely implemented (Westbrook, 2005), one main limitation of the volumetric registration is that it treats the head as a rigid-body and minimizes motion only between the acquired volumes (Murphy et al., 2013). However, in standard fast 2D MRI, each excitation pulse excites the magnetization of one slice at a time, while the head moves across all slices. This approach is therefore insensitive to the consequences of head-motion on activation timing and patterns of excitation that occur across slices during volume acquisition (Cheng & Puce, 2014).

More recently, a slice-based head-motion correction method was introduced to account also for these effects (Beall & Lowe, 2014) together with the introduction of novel acquisition sequences (Bright & Murphy, 2013; Kundu et al., 2012).

Besides retrospective head-motion correction methods, there are some fMRI acquisition factors that are relevant for head-motion during data acquisition, such as the time to acquire the full brain volume (repetition time TR) and the slice acquisition strategy (interleaved or sequential). A common approach is to acquire slices using an interleaved pattern, which allows good brain coverage having small or no gap between slices and yet avoid interference between adjacent slices that are not perfectly rectangular (cross-talking). Interleaved slice acquisition, however, is more sensitive to head-motion happening during each single volume acquisition, giving banding artifacts (Kim et al., 2008; Sladky et al., 2011). In contrast, sequential slice-order sequences present opposite characteristics and could minimize these motion-related artifacts during BOLD-weighted echo-planar imaging (EPI) volume acquisition, provided that a sufficient gap between adjacent slices is used (Kim et al., 2008; Sladky et al., 2011).

To the best of our knowledge, no studies have investigated whether there is an optimal combination of slice-order acquisition (sequential vs interleaved) and retrospective head-motion correction (volume- vs slice-based motion correction) methods that minimizes the sensitivity to in-scanner head-motion, thus giving an optimal test-retest reproducibility of intrinsic DMN connectivity. This is of interest as part of the optimization of acquisition and analyses protocols for longitudinal studies. In this study of healthy young adults, we evaluate how the combination between ascending slice acquisition methods, interleaved or sequential, and head-motion correction methods, volume-based or slice-based, influences the TRT reproducibility of intrinsic DMN connectivity metrics.

2 Materials & Methods

2.1 Subjects

24 healthy young volunteers (12 female, 27.0 ± 5.3 y) participated in this study approved by the ethical committee of the University of Trento. Subjects were scanned across two sessions, in average 4.2 ± 4.4 days apart. During each resting-state fMRI session subjects were asked to relax, keep their eyes closed, stay still while avoiding to fall asleep or engage in structured thoughts. Data from 1 participant were excluded from the analysis for being collected with a smaller number of TRs.

2.2 MR image acquisition

A 4T Bruker Medspec scanner (Bruker Medical, Ettlingen, Germany) with a birdcage-transmit and an 8-channel receive head coil (USA Instruments, Inc., Ohio) was used. In each session, one 3D T1-weighted MP-RAGE (TR/TE 2,700/4.18 ms; 1 mm^3 voxel), and two resting state fMRI runs (TR/TE 2.2s/30 ms, with 37 AC-PC parallel slices, voxel size 3x3x3 mm^3, slice-gap 0.6 mm, 200 volumes) were acquired. The resting-state runs were acquired once with ascending interleaved and once with ascending sequential 2D slice acqusition orders. Slice-order acquisitions were not counterbalanced in the present study, with sequential acquisitions always being the last data to be acquired.

There is a risk that the last data to be acquired in each session (sequential slice acquisition) would show higher fatigue effects by introducing higher motion and potentially lower temporal signal-to-noise ratio (tSNR). This could introduce a bias for the sequential acquisition that could

confound differences relative to the sequential acquisition. Such biases where evaluated by within session tSNR comparisons (see below).

2.3 Pre-processing

All DICOMs (Digital Imaging COmmunications in Medicine) were converted into Neuroimaging Informatics Technology Initiative (NIfTI) images using dicom2nii converter program in MRIcron. During conversion, 2 resting-state functional images that were acquired using the interleaved slice acquisition were inadequately flipped along the x-axis and were thus reoriented using the 3drotate AFNI tool.

The pre-processing of the functional EPI data was performed in the individual space of each subject using a combination of FSL (Jenkinson et al., 2012) and AFNI (Cox, 1996) programs (Figure 1). The first 6 volumes were discarded (fslroi, FSL) to allow for steady state stabilization of the BOLD fMRI signal. The temporal signal-to-noise ratio (tSNR) from the full brain was here estimated (194 volumes) prior to any preprocessing corrections so that it would be in principle sensitive to head-motion. The rationale was to evaluate whether potentially higher motion, due to higher fatigue during sequential acquisitions, would cause systematic reduction of tSNR.

Afterwards, either volume-based or slice-based head-motion correction methods were implemented before slice-timing correction based on the slice-order acquisition method (slicetimer, FSL). The order of these corrections is controversial (Johnstone et al., 2006) but was here consistently adopted because predefined in SLOMOCO (see section 2.4.2) (Beall & Lowe, 2014; Jones et al., 2008). From both head-motion correction methods the 6 movement parameters were calculated.

Then, non-brain voxels were removed from the EPI volume (bet2, FSL) and, to remove

high-frequency signal fluctuations, a temporal filtering with a bandpass filter (0.01 - 0.1Hz) was used on both the EPI volume (fslmaths, FSL) and the 6 head movement parameters (1dBandpass, AFNI) (Hallquist et al., 2013). Multiple linear regressions (3dDeconvolve, AFNI) were used to remove the 6 movement parameters and their relative derivatives (1d_tool.py, AFNI) plus second-order polynomials from the main signal. Individual brain volumes were normalized to mean signal intensity by a single factor of 1000 (fslmaths, FSL) and registered to brain-extracted anatomical volumes using Boundary-Based-Registration (Greve & Fischl, 2009).

FMRIB's ICA-based Xnoiseifier (FSL-FIX) (Griffanti et al., 2014; Salimi-Khorshidi et al., 2014) was implemented to classify and remove the independent spatial components (25, MELODIC) associated with physiological noise and MRI hardware-related artifacts using a standard classifier (Standard.RData: TR=3s, Resolution=3.5x3.5x3.5mm^3, session=6mins, default FEAT pre-processing) and a medium classification threshold (50/100) as a criterion to distinguish between signal and noise associated components. To remove physiological noise confounds FSL-FIX uses the non-gray matter tissue masks (CSF and white matter) and the 6 motion parameters obtained after head-motion correction. The tissue masks are derived from the brain extracted anatomical volume, which was obtained using OptiBET for each single subject and session (Lutkenhoff et al., 2014).

For each condition, all subjects and sessions were spatially normalized to the MNI template via application of linear (affine) FLIRT (Jenkinson & Smith, 2001) and subsampled at a resolution of 3 mm isotropic voxels. To evaluate data preprocessing quality, the mean tSNR was estimated (194 volumes) on the three main tissue classes (GM, WM, CSF) for each slice-order acquisition (interleaved and sequential) and each head motion correction strategy (VOMOCO and SLOMOCO).

No spatial smoothing was applied in accordance to the recommendations by FSL-FIX developers (Salimi-Khorshidi et al., 2014). This choice has been seen not to affect the detectability

of the DMN (Molloy et al., 2014). Given that ICA tends to separate motion components, we decided not to censor volumes in this study (Power et al., 2012). This also lets us use FSL-FIX and perform group analysis on time series of the same length (N=194).

2.4 Head-motion correction methods

Below we outline the two head-motion correction methods applied and compared in this study: volume-based head-motion correction, here referred to as VOMOCO (Jenkinson et al., 2002), and slice-based head-motion correction, here referred to as SLOMOCO (Beall & Lowe, 2014).

2.4.1 Volume-based head-motion correction

VOMOCO was performed using a rigid-body motion correction method (http://fsl.fmrib.ox.ac.uk/fsl/fslwiki/MCFLIRT) based on the affine registration tool in FSL (FLIRT). For each subject and session, the train of 3D brain volumes (N=194) was registered to the middle reference volume (97th) using linear sinc interpolation with 6 degrees of freedom (DOF). This procedure yields a transformation matrix of 6 volumetric movement displacement parameters.

2.4.2 Slice-based head-motion correction

SLOMOCO was performed using SLice-Oriented MOtion COrrection (http://www.nitrc.org/frs/?group_id=361). SLOMOCO is a publicly available slice-based motion regression method that corrects each slice for movement within and between volumes using AFNI programs. During within-volume motion correction each slice undergoes an in-plane co-

registration. Motion estimates are regressed from each voxel including movement information from adjacent slices. Thereafter, between-volume motion correction is performed for each slice of interest (all other slices are replaced with their mean timeseries across time). This procedure yields a 6 DOF transformation matrix re-assembling the 3 DOF movement time-series resulting from both correction steps and matching the average of their variances, respectively. Of note, time-series from between-volume correction are variance-normalized and all slices have the same variance thereof (Beall & Lowe, 2014).

2.5 Head-motion derived metrics

In order to evaluate the amount of motion estimated by the two head-motion correction methods, the transformation matrices were analyzed for each subject and session. Head rotation parameters were converted from radians to millimeters in terms of the corresponding displacement on a r=50 mm sphere, representing the average distance between cortex and head center (Siegel et al., 2014). The straight sum between the 6 parameters (in absolute value) was computed to generate a 1D timeseries here referred to as the volume-to-volume displacement, for each subject and session. To further summarize head-motion in each subject, the median volume-to-volume displacement was calculated.

2.6 Characterization of group DMN for each condition

After data preprocessing, we performed group independent component analysis (group-ICA) as implemented in the MELODIC ICA toolbox (Version 3.13) from FSL (Version 5.0.4) to extract the group DMN map relative to each combination of slice-order acquisition and head-motion correction method, respectively. All functional volumes across subjects (N=23) and sessions (N=2) were temporally concatenated and the obtained signal was decomposed into 15 independent components (Infomax algorithm). Time-courses were not variance-normalized and default

parameters were used for the mixture model fit. Dimensionality (15 ICs) was tailored to the empiric data to define the group DMN component across all conditions of interest (N=4). Qualitative evaluations showed that higher dimensionality (16-20 ICs) gave splitting of the DMN across multiple components, while lower dimensionality (10-14 ICs) was insufficient to gain optimal IC estimation (Abou Elseoud et al., 2011; Jovicich et al., 2016).

For each condition, the DMN was visually selected among the 15 components as the one that included the most common DMN nodes: medial prefrontal and anterior cingulate cortex, posterior cingulate cortex and precuneus, left/right latero-parietal cortex, using a threshold of z-score > 2.3 (Franco et al., 2010) (Figure 2A). A reference template (Rosazza et al., 2012) was also used to qualitatively verify the degree of overlap of the group component map.

2.7 Characterization of single-subject DMN

For each slice-order acquisition and head-motion correction method, dual-regression was then used to derive the single subject and session DMN (Figure 2B) from the selected group component (Beckmann et al., 2009). Individual DMN volume maps were thresholded at $z > 2.3$, $p < 0.01$ (Beckmann & Smith, 2004).

To account for spatial DMN variability across sessions and subjects a cluster analysis was run to detect the four main functional co-activated clusters that characterize the DMN (3dclust, AFNI). These clusters are the posterior cingulate and precuneus (including BA31, BA30, BA29, BA23), the left/right ventral and dorsal posterior parietal cortex (including BA39, BA40, BA22, BA7) and prefrontal and anterior cingulate areas (including BA9, BA10, BA32, BA24) (Franco et al., 2010). To avoid inaccuracies for the definition of DMN activation maps, clusters were defined as made of voxels no more than 4 mm apart and a cluster volume of at least 67 mm^3 in volume size, per each region-of-interest (ROI) (Marchitelli et al., 2016).

These clusters were anatomically constrained by a reference DMN template (Rosazza et al.,

2012). Visual inspection was done to verify that clusters overlapped with the main regions attributed to the DMN.

Mean z-scores in the DMN (i.e., the mean z-score across all voxels in the four main clusters) and relative activation cluster-size (i.e. the total number of voxels in the four main nodes) were characterized for each subject, session and condition. In addition, mean z-scores and relative cluster-size were also calculated for the posterior cingulate, medial prefrontal cortex and parietal cortex, separately.

In addition to the combined group-ICA and dual-regression analysis, we also evaluated intrinsic DMN connectivity using a ROI-based approach, considering its wide employment in functional connectivity studies (Biswal et al., 1995; Raichle et al., 2001; Fox et al., 2006; Vincent et al., 2008). The ROI-based approach used spherical ROIs (10 mm radius) derived from the same reference template used for the group-ICA and dual-regression analysis (Rosazza et al., 2011). These ROIs were located around the PCC (RAI: 0, 50, 28), ACC (RAI: 0, - 45, 17), right/left LPC (RAI: ± 47, 60, 30) on the MNI template. Of note, right/left LPCs were considered as a single ROI to be as more consistent as possible with the main ICA analysis employed in this study.

For each subject and session, completely preprocessed and co-registered to the MNI space, Pearson's correlation coefficients were calculated for each possible combination of ROI pairs and bias-corrected using a bootstrap procedure (*1dCorrelate,* AFNI). Correlation coefficients were then averaged within each subject and session to yield a single DMN value, and finally normalized to z-scores using the Fisher's r-to-z equation.

2.8 Test-retest reproducibility of the DMN and its main nodes

The main goal of this study was to evaluate the effects of different slice-order acquisition and head-motion correction methods on the longitudinal reproducibility of intrinsic DMN

connectivity. Three measures of TRT reproducibility of functional connectivity patterns were evaluated on suprathresholded z-scores DMN maps (z > 2.3) for each ROI, slice acquisition and motion correction method, respectively:

1) The absolute percentage error to measure the inter-session error in ROI-wise mean z-scores for each subject (Bennett & Miller, 2010):

$$\%\ error\ =\ \frac{\mathrm{D}(iFC)}{\mathrm{S}(iFC)/2}*100$$

with $\mathrm{D}(iFC)$ indicating the absolute difference in mean z-scores within each subject across test and retest sessions; $\mathrm{S}(iFC)/2$, indicating the average functional connectivity (mean z-score) within each subject across sessions.

2) ROI-wise intraclass correlation coefficient, ICC (2,1) (Shrout & Fleiss, 1979) of mean z-scores and relative confidence intervals (C.I.) (McGraw & Wong, 1996) to measure the proportion of inter-subject variance out of the total variance in the entire sample:

$$ICC\ (2,1)\ =\ \frac{s^{2}_{(between)}}{s^{2}_{(between)}+s^{2}_{(within)}+e}$$

with $\sigma^2_{(between)}$ and $\sigma^2_{(within)}$ indicating the inter-subject and intra-subject variance in mean z-scores, respectively and ε is the residual error;

3) To measure voxel-wise spatial reproducibility of the DMN we used for each subject the Jaccard index, here defined as the fraction between shared (intersection, $\cap$) active voxels out of all (union, $\cup$) active voxels across sessions:

$$\mathrm{J} = \frac{(\mathrm{N}^{\circ}\ \mathrm{voxels}_{(\mathrm{test})}\ \cap\ \mathrm{N}^{\circ}\ \mathrm{voxels}_{(retest)})}{(\mathrm{N}^{\circ}\ \mathrm{voxels}_{(\mathrm{test})}\ \cup\ \mathrm{N}^{\circ}\ \mathrm{voxels}_{(retest)})}$$

The Jaccard index was computed for the DMN as a whole and for each single DMN node separately (PCC, ACC, LPC and RPC), for each acquisition and head-motion correction method.

2.9 Statistical evaluations

Statistical evaluations were performed in IBM SPSS Statistics for Macintosh, Version 22.0. We used bivariate Pearson's correlations to evaluate the existence of relationships between head movement measures (i.e. median volume-to-volume displacements) and functional connectivity and its TRT reproducibility in all the ROIs (N=4) and for each combination of slice-order acquisition and head-motion correction method (N=4). Of note, when correlating TRT reproducibility scores and motion-derived metrics, median displacements were averaged across the two sessions.

We used a paired t-test to evaluate slice-order acquisition effects potentially induced by motion in the full-brain tSNR from the non-preprocessed acquired data (N=46). After data preprocessing, the non-parametric Friedman test was conducted across all subjects and sessions (N=46) to assess for significant head-motion correction and/or slice-order acquisition method effects in the mean tSNR values in GM and the other brain tissues (WM, CSF).

We performed the non-parametric Friedman test to evaluate both slice-order acquisition and head-motion correction method effects in mean gray-matter tSNR values after data preprocessing and MNI normalization (N=46). The same non-parametric test was conducted to evaluate the effects of interest on the median values of motion-derived metrics across all subjects and sessions (N=46). The Friedman test was finally used also to assess slice-order acquisition and head-motion correction method effects in mean ICA z-scores (N=46) and TRT reproducibility values (N=23), for the entire DMN and its single nodes, respectively. Correspondingly, the test was also employed for mean DMN (Fisher's z-normalized) correlation coefficients (N=46) and associated TRT reproducibility scores (N=23). A statistical comparison analysis between the group-ICA / dual

regression and the ROI-based methods was also conducted for each slice-order acquisition and head-motion correction method using a paired-samples t-test.

Statistical significance level was set to $p < 0.05$. Statistics were corrected for multiple comparisons over all possible pairwise combinations using the method of Dunn-Bonferroni (Dunn, 1964) at $\alpha = 0.05$ and C.I. = 95%.

3 Results

3.1 Head-motion estimates and tSNR evaluations

The overall estimated head-motion parameters from VOMOCO and SLOMOCO are illustrated in Figure 3A. The Friedman test performed across all slice-order acquisition and head-motion correction methods revealed significant differences in the amount of movement estimated (**Table 1**). Pairwise comparisons revealed that median displacements estimated using VOMOCO (0.19 ± 0.14 mm) were significantly lower than SLOMOCO (1.16 ± 1.44 mm) for both interleaved ($Z = -2$, $p < 0.001$) and sequential ($Z = -2$, $p < 0.001$) acquisitions.

Prior to data preprocessing, a paired sample t-test indicated no significant difference in tSNR measures for interleaved (22.2 ± 4.3) and sequential (22.6 ± 4.4) slice acquisition methods before data preprocessing; $t(45) = -4.9$, $p = 0.63$. Since the sequential slice acquisition was always the last acquisition in each session, the lack of systematic tSNR differences between the two slice acquisition methods is consistent with a lack bias that could have resulted from increased fatigue (motion) in the last run.

After data preprocessing, significant differences in tSNR were found within GM across methods (**Table 1**). Pairwise comparisons across conditions revealed that slice acquisition order had no effects on tSNR. However, SLOMOCO consistently gave higher tSNR than VOMOCO: SLOMOCO (334 ± 73), VOMOCO (276 ± 65) for both interleaved ($Z = -1.8$, $p < 0.001$) and sequential ($Z = -1.3$, $p < 0.001$) acquisitions (**Figure 3B**). Similar findings were obtained for all brain tissue classes examined (GM, WM, CSF), with tSNR percent increases in the range of 23-26% for SLOMOCO relative to VOMOCO (**Supplementary Figure 1**). The fact that the tSNR improvements offered by SLOMOCO were not specific to GM but rather general, suggests that they reflect a general reduction of the level of head motion related fluctuations.

In summary, in this group of subjects, the amount of movement estimated from both head-motion correction methods was relatively low compared to the voxel size. The movement estimates were not significantly affected by slice acquisition strategy but they were significantly affected by the head-motion correction method used, with SLOMOCO giving larger movement estimates and higher tSNR after data preprocessing.

3.2 Intrinsic DMN connectivity: Slice acquisition methods and head-motion correction effects

Despite differences in head movements estimated across retrospective motion correction methods, group-ICA revealed DMN co-activation patterns across all combinations of slice-order acquisition and head-motion correction methods (**Figure 4A**). No subject was discarded during data preprocessing due to excessive motion or data post processing since the dual-regression methodology combined with the functional clustering analysis were able to detect individual DMN maps across all subjects, sessions and conditions.

Intrinsic DMN connectivity results are reported in **Figure 4B.** Significant statistical differences in mean z-scores across slice-order acquisition and head-motion correction methods were found in the entire DMN (**Table 2**). Pairwise comparisons revealed that mean z-scores in the entire DMN were statistically different between head-motion correction methods for interleaved acquisition ($Z = 1.3$, $p < 0.001$) and between slice-order acquisition methods, using both VOMOCO ($Z = 0.08$, $p = 0.02$) and SLOMOCO ($Z = - 0.09$, $p = 0.005$).

Statistical significant effects were also found in each single node of the DMN (**Table 2**). In the PCC, pairwise comparisons revealed that mean z-scores were statistically different between slice-order acquisition methods only when implementing SLOMOCO ($Z = - 0.76$, $p = 0.03$). In the ACC, multiple pairwise comparisons revealed that mean z-scores in interleaved acquired and VOMOCO corrected data (7.0 ± 1.0) were statistically different from sequentially acquired ($Z = 1.72$, $p < 0.001$) and SLOMOCO corrected data ($Z = 1.68$, $p < 0.001$). Finally, in the LPC, mean z-

Test-Retest Reproducibility of the Intrinsic Default Mode Network: Influence of fMRI Slice-Order Acquisition and Head-Motion Correction Methods (doi: 10.1089/brain.2016.0450)
This paper has been peer-reviewed and accepted for publication, but has yet to undergo copyediting and proof correction. The final published version may differ from this proof.

scores were statistically different between slice-order acquisition methods (SLOMOCO: $Z = -0.9$, $p = 0.005$) and head-motion correction methods for interleaved acquisitions ($Z = 1.26$, $p < 0.001$).

Considering the whole DMN regions and the PCC node, no statistically significant correlation between mean z-scores and median volume-to-volume displacements were found for any slice-order acquisition and head-motion correction method. A weak correlation between these two metrics was found in both LPC and ACC (LPC/ACC: $\rho = 0.3$, $p < 0.05$) only for sequentially acquired data combined with VOMOCO (LPC) and SLOMOCO (ACC).

When considering the supplemental ROI-based analysis, by contrast to mean ICA z-scores, the mean z-normalized correlation coefficients associated with the entire DMN were not influenced by slice-order acquisition and head-motion correction methods (χ^2 (3, n = 46) = 0.47, $p = 0.93$).

To summarize, the main characteristic DMN nodes were found and had similar spatial locations in all slice acquisition and head-motion correction methods. However, the group connectivity estimations of the whole DMN and its separate main nodes were significantly affected by slice-order acquisition and head-motion correction methods.

3.3 TRT reproducibility of the DMN: slice acquisition and head-motion correction effects

The three TRT reproducibility measures of intrinsic DMN connectivity for each slice-order acquisition and head-motion correction method are shown in Figure 5. The absolute percentage error of mean z-scores, averaged across participants, and the ICC (2,1) scores are shown in the top and middle panels, respectively.

Descriptive and inferential statistical results are reported in Table 3. With regards to the reproducibility errors of the absolute percentage error, the overall error averaged across participants, slice acquisition methods and head-motion correction methods was below 8% and stable among DMN nodes (DMN: 7%; PCC: 8%; ACC: 6%; LPC: 8%) while ICCs (2,1) were overall fair, scoring 0.46, consistent among nodes (DMN: 0.47; PCC: 0.42; ACC: 0.5; LPC: 0.47).

There were no significant effects in either reproducibility errors or ICCs due to slice acquisition and head-motion correction methods (**Table 3**).

The supplemental ROI-based analysis revealed high absolute TRT reproducibility error of intrinsic DMN connectivity (28.5 ± 24)% across all slice-order acquisition and motion correction methods. Although, alike ICA, no significant effects due to slice acquisition and head-motion correction methods were found, the TRT reproducibility of intrinsic DMN connectivity was significantly lower in the ROI-based approach compared with the ICA-based methodology, in any condition of interest (**Supplementary Table 1**).

The Jaccard index (**bottom Figure 5**) was moderate for the overall DMN (40%), higher for the PCC node (51%) compared with LPC (39%) and the ACC node (30%) that scored the lowest reproducibility. The Friedman test performed across all subjects and conditions-of-interest revealed no statistically significant effects of either slice acquisition or head-motion correction method in the entire DMN but revealed statistically significant effects in all its single nodes (**Table 4**). Slice-order acquisition or motion correction method effects were not systematic across DMN regions. In particular, sequential acquisitions combined with SLOMOCO induced slightly opposite effects between anterior (ACC) and posterior (PCC) nodes yielding the lowest (21 ± 7)% and highest (64 ± 8)% spatial overlap reproducibility, respectively. Noteworthy, these effects were still observed at α level = 0.01 and C.I. = 99%. In the LPC, interleaved acquisition combined with VOMOCO statistically outperformed all other combinations of slice-order acquisition and motion correction methods. However, at α level = 0.01 and C.I. = 99%, significant differences were observed only between VOMOCO (52 ± 10)% and SLOMOCO (32 ± 9)% under interleaved acquired data ($Z = 1.17$, $p < 0.001$) while no slice-order acquisition effects survived.

Importantly, no statistically significant correlation was found between any TRT reproducibility measure and median motion displacements metrics, averaged across sessions, in any ROI and for any manipulation in the resting-state fMRI protocol.

Test-Retest Reproducibility of the Intrinsic Default Mode Network: Influence of fMRI Slice-Order Acquisition and Head-Motion Correction Methods (doi: 10.1089/brain.2016.0450)
This paper has been peer-reviewed and accepted for publication, but has yet to undergo copyediting and proof correction. The final published version may differ from this proof.

Brain Connectivity

To summarize, neither slice-order acquisition nor head-motion correction methods affected the TRT reproducibility of mean z-scores in the DMN as well as among its nodes. Nor they affected the spatial overlap reproducibility of the entire DMN. However, the spatial overlap reproducibility was subjected to inter-regional variability, with frontal DMN node (ACC) as the least spatially reproducible. The choice of interleaved slice-order acquisition yielded the most reduced inter-regional DMN variability regardless head-motion correction methods. Most importantly, no combination of slice acquisition and head-motion correction method was found that would offer significant TRT reproducibility improvements that were systematically consistent across DMN nodes.

4 Discussion

4.1 Main findings

The main goal of this TRT reproducibility study was to evaluate whether different combinations of slice-order fMRI acquisition protocols and head-motion correction techniques would differently affect the longitudinal stability of intrinsic DMN connectivity. Participants were instructed to remain as still as possible to investigate these effects in standard resting-state experimental conditions rather than with artificially directed movement. Our main findings are the following: 1) in this group of healthy young volunteers with low head-motion characteristics, group-ICA and dual-regression methodology determined robust and consistent DMN activations across all subjects (N=23) and sessions (N=2) in all conditions (N=4); 2) slice-based motion correction gave significantly higher motion estimates and also significantly higher gray matter tSNR after preprocessing; 3) slice-order acquisition and head-motion correction methods significantly affected mean z-scores in all DMN regions but they did not influence their TRT connectivity reproducibility within the same regions; 4) the spatial overlap reproducibility of DMN was also insensitive to acquisition and analysis protocol manipulations, PCC being the most and ACC the least spatially reproducible nodes, respectively; 5) most importantly, no combination of slice acquisition and head-motion correction methods improved the TRT reproducibility of intrinsic DMN connectivity in a systematic way.

4.2 Retrospective motion correction methods

In agreement with previous studies (Beall & Lowe, 2014), our results show that, on the same data, SLOMOCO systematically gives higher movement estimates compared with VOMOCO, which on average has been seen to miss at least the 50% of non-volumetric motion in real data. In

average, across all participants and sessions (N=46), SLOMOCO parameters registered 64% and 61% higher motion than VOMOCO under interleaved and sequential slice-order acquisitions, respectively. Although both methods indicated overall low motion in the data, SLOMOCO yielded significantly higher tSNR in gray matter compared with VOMOCO under both slice-order acquisitions. This finding encourages the adoption and further development of intra-volume motion correction methods to enhance existing inter-volume retrospective correction approaches in cross-sectional resting-state FC-MRI studies.

4.3 Intrinsic DMN connectivity

Using group-ICA and dual-regression methods we were able to identify the group DMN and reconstruct all individual DMN components under all slice-order acquisition and head-motion correction methods across fMRI sessions. These findings highlight the reliable nature of the ICA approach (Beckmann et al., 2009) to define stable DMN maps in longitudinal resting-state FC-MRI studies (Chen et al., 2008; Damoiseaux et al., 2006; Biswal et al., 2010; Jovicich et al., 2016).

Both slice-order acquisition and head-motion correction methods affected intrinsic DMN connectivity in the whole network and its single nodes. However, this effect was not equally distributed across all DMN nodes, being less prominent in the PCC region. In fact, in contrast to all other DMN nodes, we found that mean z-scores in the PCC were very robust against potential surviving motion artifacts, with no significant correlations with the estimated motion from both VOMOCO and SLOMOCO. These observations confirm the resilience of the main hub of the DMN (Fransson & Marrelec, 2008) and support research in PCC-based connectivity markers of dementia (Bai et al., 2009; Zhou et al., 2008).

4.4 Test-retest reproducibility of the DMN

On the contrary, neither slice-order acquisition nor head-motion correction methods affected TRT reproducibility errors or the ICCs. Both of these metrics gave fair-to-good reproducibility in mean z-scores, in agreement with previous DMN reproducibility studies (Shehzad et al., 2009; Braun et al., 2012). Importantly, both reproducibility metrics were not subjected to inter-regional variability across the main network's nodes. These findings suggest that whereas intrinsic DMN connectivity metrics are markedly sensitive to head-motion artifacts (Van Dijk et al., 2012) and relative correction choices (Power et al., 2014), the connectivity reproducibility results are comparable and robust. Despite circumscribed to a low-motion cohort, this might indicate an individual trait-like stable property of motion (Van Dijk et al., 2012) that cannot be accounted for by the evaluated slice-order acquisition and motion correction methods.

When compared with group-ICA and dual-regression, the intrinsic DMN connectivity calculated via the ROI-based approach yielded overall poorer reproducibility. This generalizes previous comparative findings (Jovicich et al., 2016) and indicates that multivariate data-driven approaches show higher capability to discriminate neural from non-neural BOLD signal sources (Beckmann et al., 2005). In particular, the selection of ROI size, shape and location across and within individuals remains challenging for longitudinal resting-state fMRI studies.

The spatial overlap reproducibility of the entire DMN was moderate and, unlike mean z-scores, insensitive to slice-order acquisition and motion correction methods. Nevertheless, it showed a certain degree of variability among DMN nodes, with the highest reproducibility in the PCC (52 ± 13)% and the lowest in the ACC (30 ± 11)%. This finding is in agreement with previous 3T studies that found higher variability in frontal DMN areas across subjects and sessions (Van Dijk et al., 2010, Damoiseaux et al., 2006).

We found that none of the DMN reproducibility measures correlated with motion-derived parameters or were influenced by slice-order acquisition or head-motion correction

methods. This null effect could be a consequence of the low head-motion parameters in our participants. A different protocol could have been considered in which subjects were asked to follow particular patterns of head-motion to then parametrically characterize their effects on the acquisition and preprocessing schemes (Reuter et al, 2015). Such a study, however, would have no longer been a resting state study and we decided to acquire our data using classical instructions as done in the vast majority of resting-state acquisitions. Other studies have shown that higher levels of head-motion can negatively influence the TRT reproducibility of the DMN in healthy elders, acquired using interleaved sequences and applying VOMOCO methods (Guo et al., 2012).

4.5 Limitations and future directions

This study presents several limitations. As previously mentioned, the low levels of head motion in our population might have hidden significant acquisition and/or correction method effects in the reproducibility of the DMN. Populations prone to higher degree of head motion might be of interest for further studies. The data-driven strategy here implemented using ICA could be an additional reason for having found that reproducibility was invariant to the factors manipulated. Not only ICA is known to give reproducible components (Abou Elseoud et al., 2011; Calhoun et al., 2009; Zuo et al., 2010) but it was also used twice in our workflow, using the ICA-based method FSL-FIX to remove physiological noise and surviving motion-related signals (Griffanti et al., 2014; Salimi-Khorshidi et al., 2014). This double ICA decomposition could have helped reduce the amount of motion-related variability investigated. Besides ICA, there are alternative methods for estimating DMN connectivity. In particular, a widely used method is seed-based connectivity with a seed positioned in the PCC (Andrews-Hanna et al., 2012; Buckner et al., 2008; Fransson and Marrelec, 2008). Although known for its robust results, this method is prone to lower reproducibility because it relies on the use of the PCC anatomical prior, typically taken from an anatomical atlas. ICA, on the other hand, being data-driven, is potentially better suited at removing signal fluctuations that are unrelated to the DMN activity that could reduce TRT reproducibility. In

fact, a recent study directly compared ICA and seed-based DMN showing that the ICA test-retest reproducibility was superior (Jovicich et al., 2016).

Other limitations are related to data acquisition: this DMN reproducibility study is that the order of sequential and interleaved slice acquisitions was not counterbalanced across subjects and sessions. Instead, sequential acquisition was systematically the last run in every session for all subjects. This raises the possibility of biases, given that fatigue effects could make the subjects systematically move more during the last session, giving both higher motion metrics and potentially lower tSNR for the sequential slice acquisition protocol. Our evaluations show, however, that there were neither significant systematic motion metrics nor tSNR differences between the two acquisitions in each run. Also, we used an ascending protocol for both slice acquisition methods. Using descending protocols would have potentially made the data more robust against blood in-flow saturation effects in that direction (Turner et al., 1998), with overall lower sensitivity to motion spin-history artifacts.

Finally, this reproducibility study only investigates one resting-state network: the DMN. While other resting state networks are of interest too, our data-driven approach was tailored to characterize this network and might show weaknesses when examining the entire functional connectome. While other group-ICA algorithms could be further evaluated to characterize reproducibility and head motion sensitivity (Esposito et al., 2005; Goebel et al., 2006), more and more FC-MRI studies are using graph-theoretical measurements (van den Heuvel and Sporns, 2013; Sporns, 2014) to investigate the architecture of resting-state networks, and may offer improved reproducibility (Braun et al., 2012); future studies should therefore also investigate how acquisition and preprocessing choices might influence the TRT reproducibility of graph-derived metrics.

To address this limitation, we make the raw test-retest data of this study (24 subjects, each with two slice acquisitions and two sessions, making a total of 96 resting state fMRI datasets) publicly available at The Consortium for Reliability and Reproducibility (Zuo et al., 2014). Sharing the data may facilitate the evaluation of additional retrospective head-motion correction methods,

additional resting state networks and additional connectivity metrics. Other analysis software and group-ICA algorithms could be further evaluated to characterize reproducibility and head motion sensitivity (Esposito et al., 2005; Goebel et al., 2006).

Brain Connectivity
Test-Retest Reproducibility of the Intrinsic Default Mode Network: Influence of fMRI Slice-Order Acquisition and Head-Motion Correction Methods (doi: 10.1089/brain.2016.0450)
This paper has been peer-reviewed and accepted for publication, but has yet to undergo copyediting and proof correction. The final published version may differ from this proof.

5 Conclusions

This work evaluates how interleaved or sequential ascending slice-order acquisitions combined with volume-based or slice-based retrospective head-motion correction methods influence the short-term TRT reproducibility of the intrinsic DMN reproducibility in a group of healthy young adults. Both motion correction methods detected overall low motion, with slice-based detecting systematically higher motion than volumetric-based correction and higher gray matter tSNR (21%). Group-ICA and dual-regression methods were able to reliably characterize the DMN in the entire sample across all these fMRI protocol manipulations. The intrinsic DMN connectivity was sensitive to protocol manipulations but the TRT reproducibility of the DMN was not. Both inter-session percentage errors (8%) and the ICC analysis (ICC = 0.47) indicate fair-to-good reproducibility of mean z-scores while the Jaccard index indicates moderate spatial overlap reproducibility (40%) of the DMN. The TRT reproducibility of mean z-scores is constant between the main DMN nodes (PCC, LPC and ACC) across all slice acquisition and motion correction methods. In contrast, the spatial overlap reproducibility is the highest in the PCC (52 ± 13)% and the lowest in the ACC (30 ± 11)%. None of the four protocols evaluated gave a systematic improvement of reproducibility relative to the others. Our findings, limited to a population with low head-motion characteristics, suggest that for longitudinal studies the four protocols evaluated offer comparable sensitivity to detect longitudinal effects. However, for cross-sectional studies our findings suggest that controlling for consistency in slice acquisition and motion correction methods is important because these can bias the intrinsic connectivity estimates.

Acknowledgments

Special thanks to Giulia Elli for resting-state data acquisition and to the CiMEC MRI laboratory for medical and technical support. Research was supported in part by a European Research Council starting grant (MADVIS; ERC-StG 337573) attributed to O. Collignon.

Disclosure Statement

No competing financial interests exist.

List of Figures

Figure 1

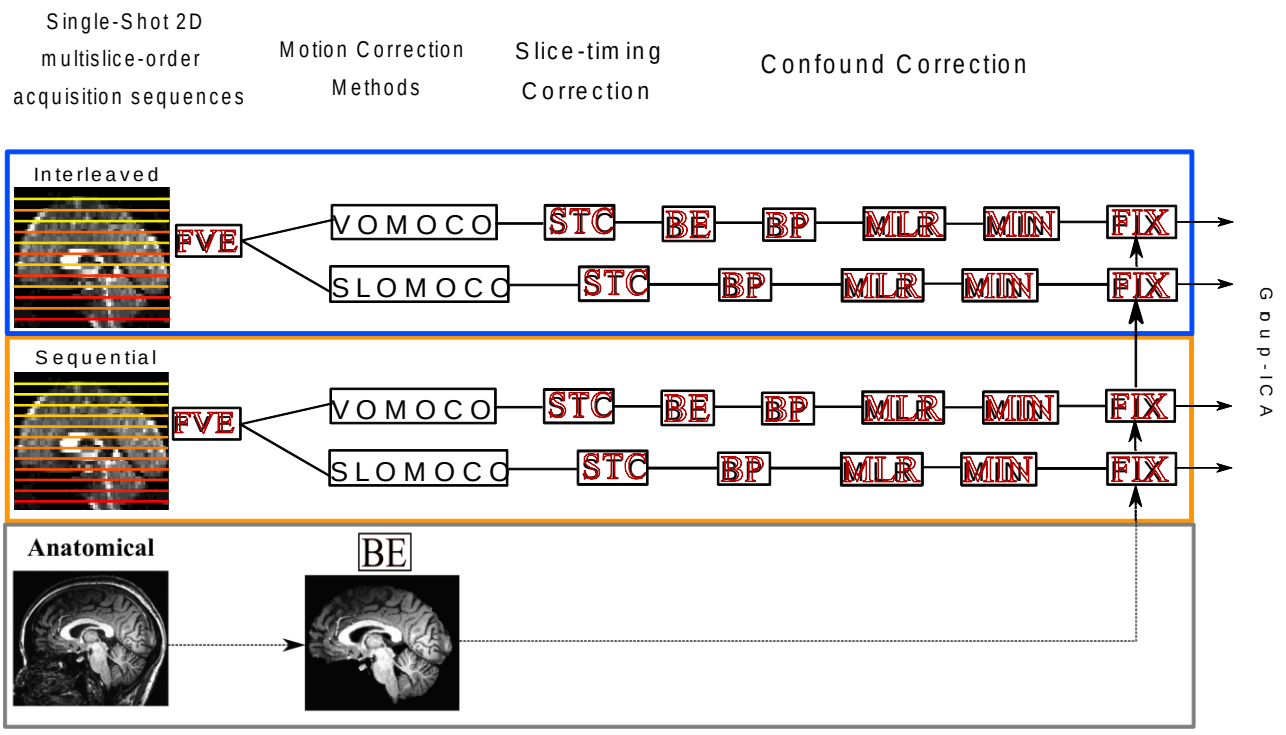

Test-Retest Reproducibility of the Intrinsic Default Mode Network: Influence of fMRI Slice-Order Acquisition and Head-Motion Correction Methods (doi: 10.1089/brain.2016.0450)
This paper has been peer-reviewed and accepted for publication, but has yet to undergo copyediting and proof correction. The final published version may differ from this proof.

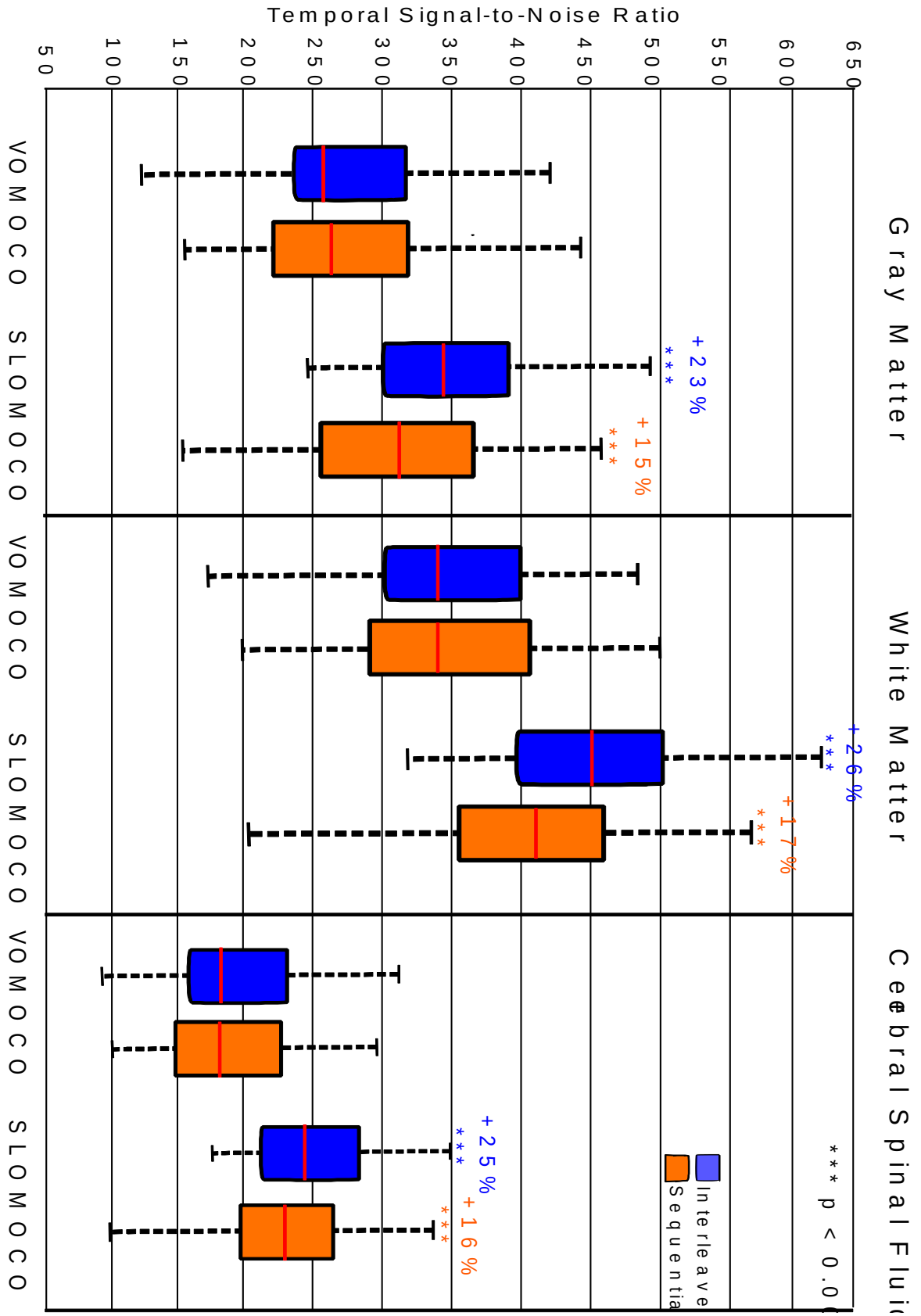

Figure 1. Pre-processing workflow. The figure illustrates the pre-processing pipeline under each slice-order acquisition condition, either interleaved (blue rectangle) or sequential

(orange rectangle) and motion correction method, either volume-based (VOMOCO) or slice-based (SLOMOCO). FVE, denotes the removal of the first 6 volumes from the BOLD timeseries; STC, slice-timing correction (interleaved / sequential); BE, brain extraction (included in SLOMOCO); BP = band-pass filtering (0.01–0.1 Hz); MLR, multiple linear regression (12 head movement timeseries (6 head movement timeseries + 6 derivatives) filtered as BP; MIN, mean intensity normalization; FIX, FSL-FIX implementation. The bottom row indicates the anatomical brain extraction step needed for use in FSL-FIX (see text for more details).

Figure 2

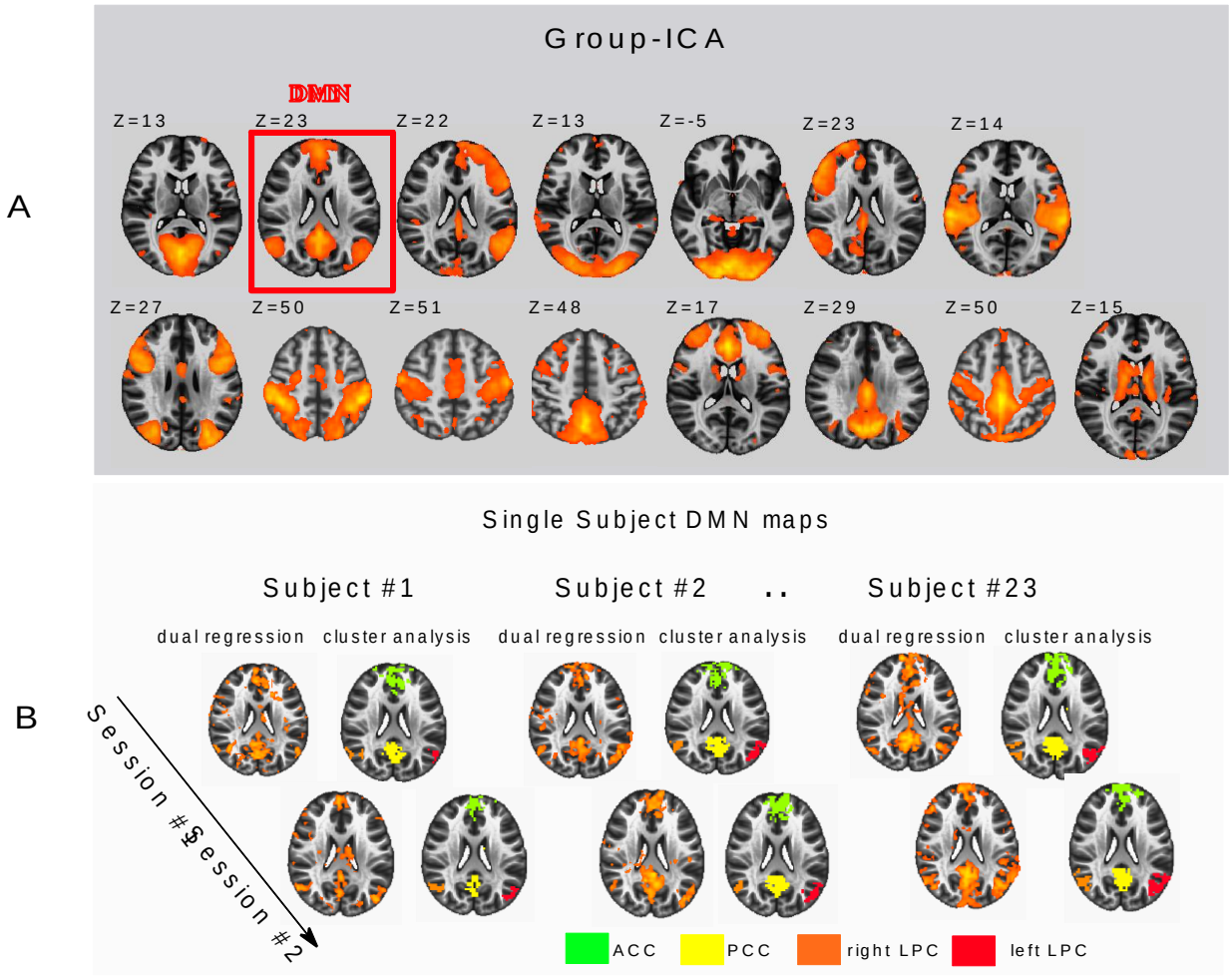

Figure 2. Group-ICA and Dual Regression Analysis. The figure illustrates (A) sample group-ICA results (Interleaved + SLOMOCO) using 15 components on the group of 46 subjects. Statistical maps were thresholded at z > 2.3. The second component in the top-left corner was visually selected as the DMN in this example (red rectangle). (B) For the same conditions (Interleaved + SLOMOCO), dual regression results relative to the DMN across sample subjects (columns) and sessions (rows) are here shown in statistical maps thresholded at z > 2.3 (left column). The ultimate individual regions detected using the cluster analysis and forwarded to TRT reproducibility analysis are also shown next to each dual-regressed dataset. Individual DMN regions are highlighted with different colors PCC, yellow; left/right LPC, red/orange; ACC, green. MNI coordinates for the DMN: z = 23.

Figure 3

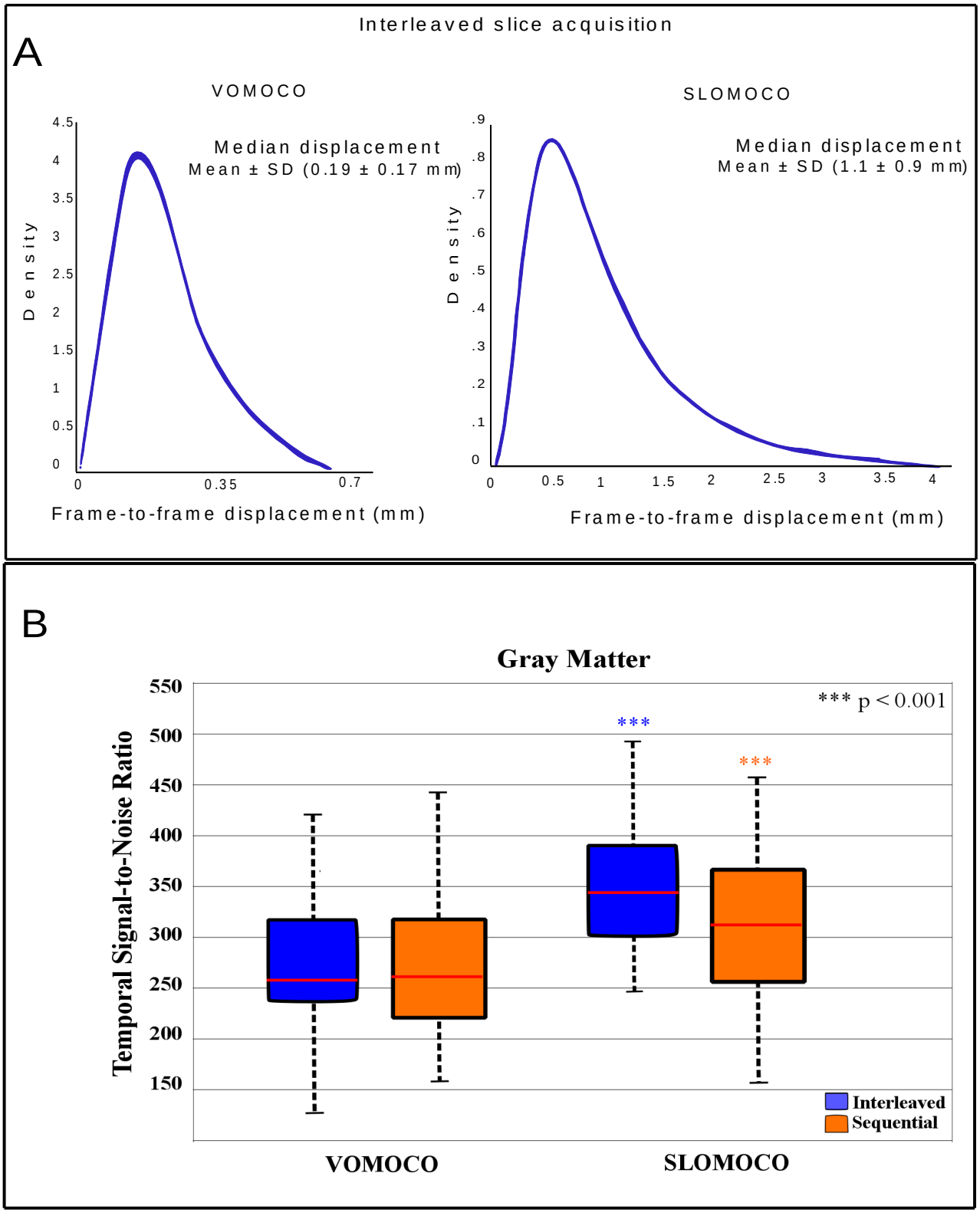

Figure 3. Overall head movement and tSNR estimates. (A) Generalized extreme value functions display the overall amount of head movement in the entire dataset, across all time points

(N=194), sessions (N=2) and subjects (N=23). VOMOCO and SLOMOCO estimates are displayed in the left and right panels, respectively. SLOMOCO returned higher movement estimates than VOMOCO. Head-motion estimates were similar across slice-order acquisitions; here the interleaved order is shown. (B) The boxplot shows the average tSNR within gray matter after data pre-processing across subjects and sessions, for each slice acquisition and motion correction method. SLOMOCO increased tSNR when compared to VOMOCO, regardless slice-order acquisition. On each box, the central red mark is the median, the edges of the box are the 25th and 75th percentiles, the dotted lines extend to the most extreme data points that are not outliers.

Figure 4

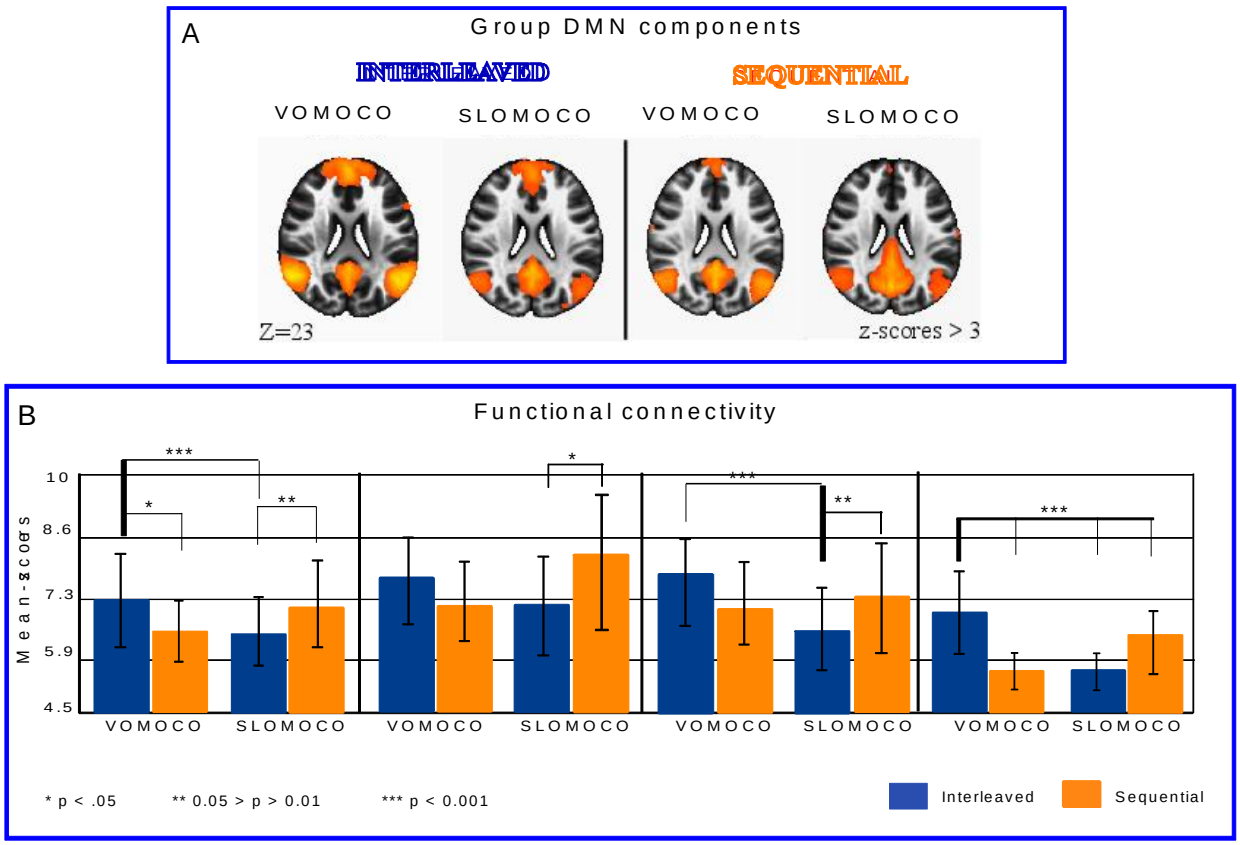

Figure 4. Group and individual intrinsic DMN connectivity. (A) Visually selected DMN components across slice acquisition (interleaved and sequential) and motion correction (VOMOCO and SLOMOCO) methods, thresholded at z > 3 for visualization purposes. The group DMN components were detected under all acquisition and analysis MRI protocols. MNI coordinates: z = 23. (B) Mean z-scores averaged across subjects and sessions (error bars are the standard deviation between subjects) in the four interrogated ROIs (from left to right): the entire DMN (DMN), the posterior cingulate cortex (PCC), lateroparietal lobes (LPC), and anterior cingulate (ACC). For each ROI, results are differentiated for motion correction method, within which slice-order conditions are displayed (Interleaved, blue; Sequential, orange). Mean z-scores are sensitive to slice acquisition and motion correction methods in all ROIs (corrected).

Figure 5

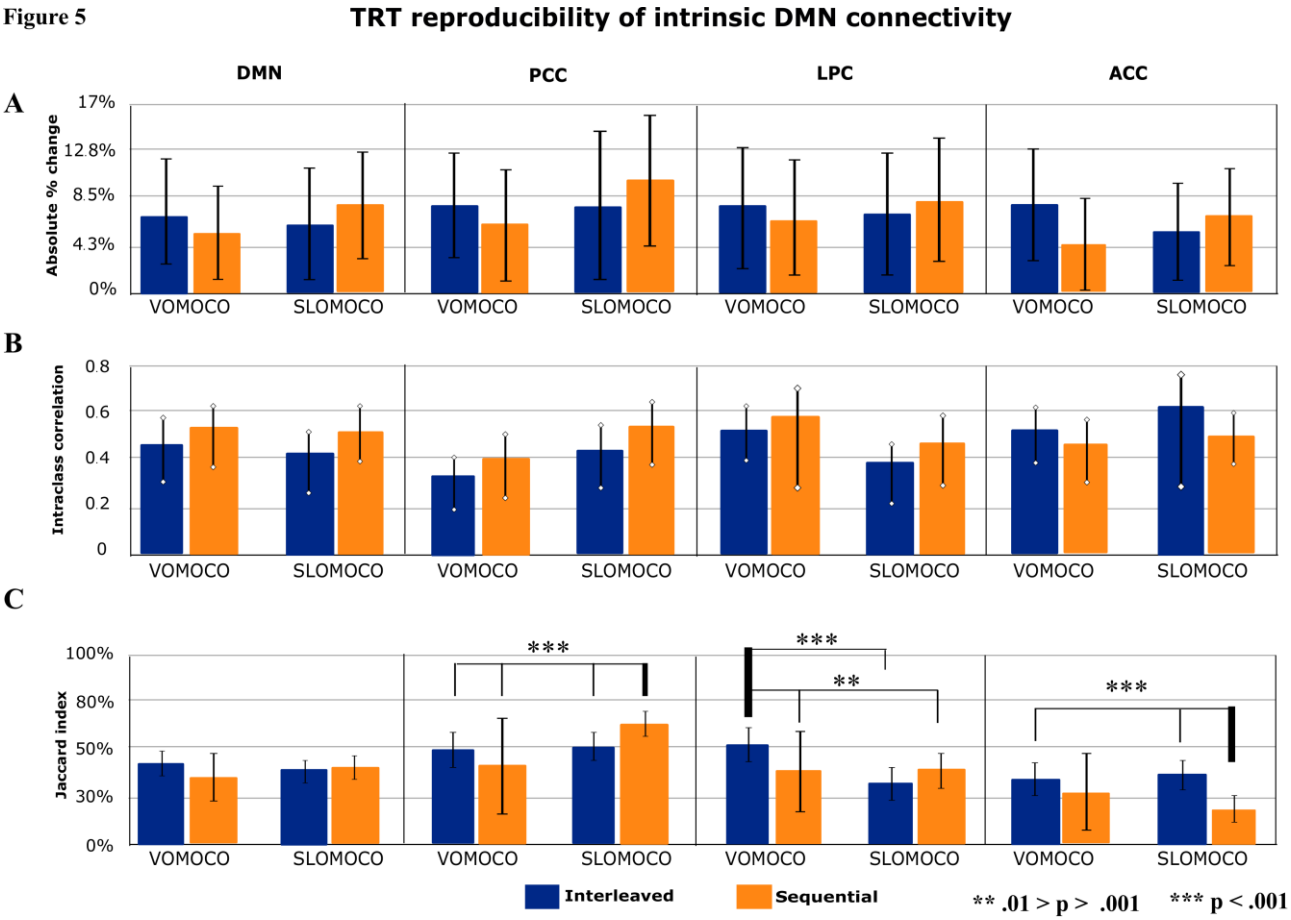

Figure 5. Test-retest reproducibility of FC-FMRI in the DMN. The figure shows (A) mean TRT reproducibility errors (error bars are the standard deviation between subjects) for mean z-scores; (B) intraclass correlation coefficients (bars indicate the confidence intervals) and (C) mean Jaccard index (error bars are the standard deviation between subjects). Results are displayed for the four interrogated ROIs (from left to right): the entire DMN (DMN), the posterior cingulate cortex (PCC), latero-parietal lobes (LPC), and anterior cingulate cortex (ACC). For each ROI, bar groups show results for each motion correction method, VOMOCO and SLOMOCO, and within each bar group, results are displayed for each slice acquisition method (Interleaved, blue; Sequential, orange). None of the reproducibility metrics indicate slice acquisition and motion correction method effects in the entire DMN. Moreover, in (A) and (B), TRT reproducibility of mean z-scores was not sensitive to these fMRI protocol manipulations in any DMN node. The TRT reproducibility of spatial overlap of single DMN regions was more sensitive to these manipulations

(corrected with Dunn-Bonferroni) and is notably reduced in the ACC in all conditions.

Supplementary Figure 1. tSNR analysis for each brain tissue. The boxplot shows the average tSNR across all subjects and sessions after data pre-processing within gray matter (left panel), white matter (middle panel) and cerebral spinal fluid (right panel). For each brain compartment, tSNR values are presented for both interleaved (blue box) and sequential (orange box) acquisitions and grouped for motion correction method (VOMOCO and SLOMOCO). Stars ($p < 0.001$, Dunn-Bonferroni corrected) on the boxes indicate that SLOMOCO, compared to VOMOCO, significantly increased tSNR for both slice-order acquisition methods and in every brain tissue. No statistically significant difference in tSNR values that could be associated with slice-order acquisition methods was observed in any brain tissue. On each box, the central red mark is the median, the edges of the box are the 25th and 75th percentiles, and dotted lines extend to the most extreme data points that are not outliers. Atop, the percent increment rate due to the application of SLOMOCO (compared with VOMOCO) is shown.

References

Abou Elseoud, A., Littow, H., Remes, J., Starck, T., Nikkinen, J., Nissilä, J., Timonen, M., Tervonen, O., Kiviniemi, V. (2011). Group-ICA Model Order Highlights Patterns of Functional Brain Connectivity. Frontiers in Systems Neuroscience, 5, 37.

Andrews-Hanna, J. R. (2012). The brain's default network and its adaptive role in internal mentation. *Neuroscientist*, *18(3)*, 251-270.

Bai, F., Watson, D. R., Yu, H., Shi, Y., Yuan, Y., & Zhang, Z. (2009). Abnormal resting-state functional connectivity of posterior cingulate cortex in amnestic type mild cognitive impairment. Brain Research, 1302, 167–74.

Balthazar, M. L., de Campos, B. M., Franco, A. R., Damasceno, B. P., & Cendes, F. (2014). Whole cortical and default mode network mean functional connectivity as potential biomarkers for mild Alzheimer's disease. *Psychiatry Res*, *221(1)*, 37-42.

Beall, E. B., & Lowe, M. J. (2014). NeuroImage SimPACE: Generating simulated motion corrupted BOLD data with synthetic-navigated acquisition for the development and evaluation of SLOMOCO : A new, highly effective slicewise motion correction. NeuroImage, 101, 21–34.

Beckmann, C. F., & Smith, S. M. (2004). Probabilistic Independent Component Analysis for Functional Magnetic Resonance Imaging. IEEE Transactions on Medical Imaging, 23, 137–152.

Beckmann, C. F., DeLuca M., Devlin J. T., Smith S. M. (2005). Investigations into resting-state connectivity using independent component analysis. Philos T Roy Soc B 360:1001-1013.

Beckmann, C. F., Mackay, C. E., Filippini, N., & Smith, S. M. (2009). Group comparison of resting-state FMRI data using multi-subject ICA and dual regression. *Neuroimage*, *47* (Suppl.1), S148.

Binnewijzend, M. A., Schoonheim, M. M., Sanz-Arigita, E., Wink, A. M., van der Flier, W. M.,

Tolboom, N., Adriaanse, S. M., Damoiseaux, J. S., Scheltens, P., van Berckel, B. N., Barkhof, F. (2012). Resting-state fMRI changes in Alzheimer's disease and mild cognitive impairment. *Neurobiol Aging, 33(9)*, 2018-28.

Biswal, B., Yetkin, F. Z., Haughton, V. M., & Hyde, J. S. (1995). Functional connectivity in the motor cortex of resting human brain using echo-planar MRI. *Magn. Reson. Med., 34*, 537– 41.

Biswal, B. B., Mennes, M., Zuo X. N., Gohel, S., Kelly, C., Smith, S. M., Beckmann, C. F., Adelstein, J. S., Buckner, R. L., Colcombe, S., Dogonowski, A.M., Ernst, M., Fair, D., Hampson, M., Hoptman, M. J., Hyde, J. S., Kiviniemi, V. J., Kötter, R., Li, S. J., Lin, C. P., Lowe, M. J., Mackay, C., Madden, D. J., Madsen, K. H., Margulies, D. S., Mayberg, H. S., McMahon, K., Monk, C. S., Mostofsky, S. H., Nagel, B. J., Pekar, J. J., Peltier, S. J., Petersen, S. E., Riedl, V., Rombouts, S. A., Rypma, B., Schlaggar, B. L., Schmidt, S., Seidler, R. D., Siegle, G. J., Sorg, C., Teng, G. J., Veijola, J., Villringer, A., Walter, M., Wang, L., Weng, X. C., Whitfield-Gabrieli, S., Williamson, P., Windischberger, C., Zang, Y. F., Zhang, H. Y., Castellanos, F. X., Milham, M. P. (2010). Toward discovery science of human brain function. *Proc. Natl. Acad. Sci. U.S.A., 107(10)*: 4734-9.

Bright, M. G., & Murphy, K. (2013). Removing motion and physiological artifacts from intrinsic BOLD fluctuations using short echo data. NeuroImage, 64, 526–537.

Braun, U., Plichta, M.M., Esslinger, C., Sauer, C., Haddad, L., Grimm, O., Mier, D., Mohnke, S., Heinz, A., Erk, S., Walter, H., Seiferth, N., Kirsch, P., Meyer-Lindenberg, A. (2012). Test-retest reliability of resting-state connectivity network characteristics using fMRI and graph theoretical measures. *Neuroimage, 59(2)*, 1404-12.

Buckner, R. L. (2012). The serendipitous discovery of the brain's default network. *Neuroimage, 62(2)*, 1137–1145.

Buckner, R. L., Andrews-Hanna, J. R., & Schacter, D. L. (2008). The brain's default network: anatomy, function, and relevance to disease. *Ann N Y Acad Sci, 1124*, 1-38.

Buckner, R. L., & Carroll, D. C. (2007). Self-projection and the brain. *Trends Cogn Sci, 11(2)*, 49-57.

Calhoun, V. D., Liu, J., & Adalı, T. (2009). A review of group-ICA for fMRI data and ICA for joint inference of imaging, genetic, and ERP data. *Neuroimage, 45(1)*, S163-S172.

Chen, S., Ross, T. J., Zhan, W., Myers, C. S., Chuang, K. S., Heishman, S. J., Stein, E. A., Yang, Y. (2008). Group independent component analysis reveals consistent resting-state networks across multiple sessions. Brain Research, 1239, 141–151.

Cheng, H., & Puce, A. (2014). Reducing respiratory effect in motion correction for EPI images with sequential slice acquisition order. Journal of Neuroscience Methods, 227, 83–9.

Cox, R. W. (1996). AFNI: software for analysis and visualization of functional magnetic resonance neuroimages. Computers and Biomedical Research, an International Journal, 29, 162–173.

Damoiseaux, J. S. (2012). Resting-state fMRI as a biomarker for Alzheimer's disease? *Alzheimers Res Ther, 4(2)*, 8.

Damoiseaux, J. S., Rombouts, S. A. R. B., Barkhof, F., Scheltens, P., Stam, C. J., Smith, S. M., & Beckmann, C. F. (2006). Consistent resting-state networks across healthy subjects. *Proc. Natl. Acad. Sci. U.S.A.*, 103, 13848–13853.

Davey, C. G., Harrison, B. J., Yücel, M., & Allen, N. B. (2012). Regionally specific alterations in functional connectivity of the anterior cingulate cortex in major depressive disorder. *Psychological medicine*, *42(10)*, 2071-2081.

Dunn, O. J. (1964). Multiple Comparisons Using Rank Sums. Technometrics, *6(3)*, pp. 241–252.

Esposito, F., Scarabino, T., Hyvarinen, A., Himberg, J., Formisano, E., Comani, S., Tedeschi, G., Goebel, R., Seifritz, E. & Di Salle, F. (2005). Independent component analysis of fMRI group studies by self-organizing clustering, *Neuroimage*, *25*, 193-205.

Fox, M. D., Corbetta, M., Snyder, A. Z., Vincent, J. L., Raichle, M. E. (2006). Spontaneous

neuronal activity distinguishes human dorsal and ventral attention systems. *Proc Natl Acad Sci U S A, 103,* 10046–51.

Franco, A. R., Pritchard, A., Calhoun, V. D., & Mayer, A. R. (2010). Interrater and intermethod reliability of default mode network selection. *Human Brain Mapping,* 30*(7),* 2293–2303.

Fransson, P., & Marrelec, G. (2008). The precuneus/posterior cingulate cortex plays a pivotal role in the default mode network: Evidence from a partial correlation network analysis. NeuroImage, 42, 1178–1184.

Godenschweger, F., Kägebein, U., Stucht, D., Yarach, U., Sciarra, A., Yakupov, R., Lüsebrink, F., Schulze, P., Speck, O. (2016). Motion correction in MRI of the brain. *Physics in medicine and biology, 61*(*5*), R32-56.

Goebel, R., Esposito, F., and Formisano, E. Analysis of FIAC data with BrainVoyager QX: From single-subject to cortically aligned group GLM analysis and self-organizing group ICA. *Human Brain Mapping, 27(5):* 392–401, 2006.

Greicius, M. D., & Menon, V. (2004). Default-mode activity during a passive sensory task: uncoupled from deactivation but impacting activation. *J Cogn Neurosci, 16(9),* 1484-1492.

Greicius, M. D., Srivastava, G., Reiss, A. L., & Menon, V. (2004). Default-mode network activity distinguishes Alzheimer's disease from healthy aging: evidence from functional MRI. *Proc. Natl. Acad. Sci. U.S.A., 101(13),* 4637-4642.

Greicius, M. D., Krasnow, B., Reiss, A. L., & Menon, V. (2003). Functional connectivity in the resting brain: a network analysis of the default mode hypothesis. *Proc Natl Acad Sci U S A, 100*(1), 253-258.

Greve, D. N., & Fischl, B. (2009). Accurate and robust brain image alignment using boundary-based registration. NeuroImage, 48(1), 63–72.

Griffanti, L., Salimi-Khorshidi, G., Beckmann, C. F., Auerbach, E. J., Douaud, G., Sexton, C. E.,

Zsoldos, E., Ebmeier, K. P., Filippini, N., Mackay, C. E., Moeller, S., Xu, J., Yacoub, E., Baselli, G., Ugurbil, K., Miller, K. L., Smith, S. M. (2014). ICA-based artefact removal and accelerated fMRI acquisition for improved resting state network imaging. NeuroImage, 95, 232–247.

Guo, C. C., Kurth, F., Zhou, J., Mayer, E. a, Eickhoff, S. B., Kramer, J. H., & Seeley, W. W. (2012). One-year test-retest reliability of intrinsic connectivity network fMRI in older adults. NeuroImage, 61*(4)*, 1471–83.

Hallquist, M. N., Hwang, K., & Luna, B. (2013). The nuisance of nuisance regression: Spectral misspecification in a common approach to resting-state fMRI preprocessing reintroduces noise and obscures functional connectivity. NeuroImage, 82, 208–225.

Hawellek, D. J., Hipp, J. F., Lewis, C. M., Corbetta, M., & Engel, A. K. (2011). Increased functional connectivity indicates the severity of cognitive impairment in multiple sclerosis. *Proc. Natl. Acad. Sci. U.S.A., 108(47)*, 19066-19071.

Hedden, T., Van Dijk, K. R., Becker, J. A., Mehta, A., Sperling, R. A., Johnson, K. A., & Buckner, R. L. (2009). Disruption of functional connectivity in clinically normal older adults harboring amyloid burden. *J Neurosci, 29(40)*, 12686-12694.

Jenkinson, M., Bannister, P., Brady, J. M. and Smith, S. M. (2002). Improved Optimisation for the Robust and Accurate Linear Registration and Motion Correction of Brain Images. *Neuroimage, 17*(2), 825-841.

Jenkinson, M., & Smith, S. (2001). A global optimisation method for robust affine registration of brain images. Medical Image Analysis, *5(2)*, 143–156.

Johnstone, T., Ores Walsh, K. S., Greischar, L. L., Alexander, A. L., Fox, A. S., Davidson, R. J., & Oakes, T. R. (2006). Motion correction and the use of motion covariates in multiple-subject fMRI analysis. Human Brain Mapping, *27(10)*, 779–788.

Jones, T. B., Bandettini, P. A., & Birn, R. M. (2008). Integration of motion correction and physiological noise regression in fMRI. NeuroImage, 42*(2)*, 582–590.

Jovicich, J., Minati, L., Marizzoni, M., Marchitelli, R., Sala-Llonch, R., Bartrés-Faz, D., Arnold, J., Benninghoff, J., Fiedler, U., Roccatagliata, L., Picco, A., Nobili, F., Blin, O., Bombois, S., Lopes, R., Bordet, R., Sein, J., Ranjeva, J. P., Didic, M., Gros-Dagnac, H., Payoux, P., Zoccatelli, G., Alessandrini, F., Beltramello, A., Bargalló, N., Ferretti, A., Caulo, M., Aiello, M., Cavaliere, C., Soricelli, A., Parnetti, L., Tarducci, R., Floridi, P., Tsolaki, M., Constantinidis, M., Drevelegas, A., Rossini, P. M., Marra, C., Schönknecht, P., Hensch, T., Hoffmann, K. T., Kuijer, J. P., Visser, P. J., Barkhof, F., Frisoni, G. B.; PharmaCog Consortium. (2016). Longitudinal reproducibility of default-mode network connectivity in healthy elderly participants: a multicentric resting-state fMRI study. *Neuroimage*, *124(PtA)*: 442-54.

Kim, B., Yeo, D. T. B., & Bhagalia, R. (2008). Comprehensive mathematical simulation of functional magnetic resonance imaging time series including motion-related image distortion and spin saturation effect. Magnetic Resonance Imaging, *26*, 147–159.

Kundu, P., Inati, S. J., Evans, J. W., Luh, W. M., & Bandettini, P. A. (2012). Differentiating BOLD and non-BOLD signals in fMRI time series using multi-echo EPI. *Neuroimage, 60(3)*, 1759–1770.

Lutkenhoff, E. S., Rosenberg, M., Chiang, J., Zhang, K., Pickard, J. D., Owen, A. M., & Monti, M. M. (2014). Optimized Brain Extraction for Pathological Brains (optiBET). PloS One, *9(12)*, e115551.

Marchitelli, R., Minati, L., Marizzoni, M., Bosch, B., Bartrés-Faz, D., Müller, B. W., Wiltfang, J., Fiedler, U., Roccatagliata, L., Picco, A., Nobili, F., Blin, O., Bombois, S., Lopes, R., Bordet, R., Sein, J., Ranjeva, J. P., Didic, M., Gros-Dagnac, H., Payoux, P., Zoccatelli, G., Alessandrini, F., Beltramello, A., Bargalló, N., Ferretti, A., Caulo, M., Aiello, M., Cavaliere,

C., Soricelli, A., Parnetti, L., Tarducci, R., Floridi, P., Tsolaki, M., Constantinidis, M., Drevelegas, A., Rossini, P. M., Marra, C., Schönknecht, P., Hensch, T., Hoffmann, K. T., Kuijer, J. P., Visser, P. J., Barkhof, F., Frisoni, G. B., Jovicich, J. (2016). Test-retest reliability of the default mode network in a multi-centric fMRI study of healthy elderly: Effects of data-driven physiological noise correction techniques. *Human Brain Mapping, 37(6):* 2114-32.

McGraw, K. O., & Wong, S. P. (1996). Forming inferences about some intraclass correlation coefficients. *Psychological methods*, *1(1)*, 30.

Molloy, E. K., Meyerand, M. E., & Birn, R. M. (2014). The influence of spatial resolution and smoothing on the detectability of resting-state and task fMRI. NeuroImage, 86, 221–230.

Mulders, P. C., van Eijndhoven, P. F., Schene, A. H., Beckmann, C. F., & Tendolkar, I. (2015). Resting-state functional connectivity in major depressive disorder: A review. *Neurosci. Biobehav. Rev. 56*, 330-344.

Murphy, K., Birn, R. M., & Bandettini, P. A. (2013). Resting-state fMRI confounds and cleanup. NeuroImage, 80, 349–359.

Power, J. D., Barnes, K. A., Snyder, A. Z., Schlaggar, B. L., & Petersen, S. E. (2012). Spurious but systematic correlations in functional connectivity MRI networks arise from subject motion. NeuroImage, 59, 2142–2154.

Power, J. D., Mitra, A., Laumann, T. O., Snyder, A. Z., Schlaggar, B. L., & Petersen, S. E. (2014). Methods to detect, characterize, and remove motion artifact in resting state fMRI. NeuroImage, 84, 320–341.

Pruim, R. H. R., Mennes, M., van Rooij, D., Llera Arenas, A., Buitelaar, J. K., & Beckmann, C. F. (2014). ICA-AROMA: A robust ICA-based strategy for removing motion artifact from fMRI data. Neuroimage, 112, 267–277.

Raichle, M. E., MacLeod, A. M., Snyder, A. Z., Powers, W. J., Gusnard, D. A., Shulman, G. L.

(2001). A default mode of brain function. Proc Natl Acad Sci U S A. 98 (2):676-82.

Reuter, M., Tisdall, M. D., Qureshi, A., Buckner, R. L., Van der Kouwe, A. J., Fischl, B. (2015). Head-motion during MRI acquisition reduces gray matter volume and thickness estimates. *Neuroimage, 107*: 107-15.

Rosazza, C., Minati, L., Ghielmetti, F., Mandelli, M. L., & Bruzzone, M. G. (2012). Functional connectivity during resting-state functional MR imaging: study of the correspondence between independent component analysis and region-of-interest-based methods. AJNR. American Journal of Neuroradiology, 33, 180–7.

Salimi-Khorshidi, G., Douaud, G., Beckmann, C. F., Glasser, M. F., Griffanti, L., & Smith, S. M. (2014). Automatic denoising of functional MRI data: Combining independent component analysis and hierarchical fusion of classifiers. NeuroImage, 90, 449–468.

Satterthwaite, T. D., Elliott, M. A., Gerraty, R. T., Ruparel, K., Loughead, J., Calkins, M. E., Eickhoff, S. B., Hakonarson, H., Gur, R. C., Gur, R. E., Wolf, D. H. (2013). An improved framework for confound regression and filtering for control of motion artifact in the preprocessing of resting-state functional connectivity data. NeuroImage, 64, 240–56.

Satterthwaite, T. D., Wolf, D. H., Loughead, J., Ruparel, K., Elliott, M. A., Hakonarson, H., Gur, R. C., Gur, R. E.. (2012). Impact of in-scanner head-motion on multiple measures of functional connectivity: Relevance for studies of neurodevelopment in youth. NeuroImage, 60, 623–632.

Schöpf, V., Kasess, C. H., Lanzenberger, R., Fischmeister, F., Windischberger, C., & Moser, E. (2010). Fully exploratory network ICA (FENICA) on resting-state fMRI data. Journal of Neuroscience Methods, 192(2), 207–213.

Schöpf, V., Windischberger, C., Robinson, S., Kasess, C. H., Fischmeister, F. P., Lanzenberger, R., Albrecht, J., Kleemann, A. M., Kopietz, R., Wiesmann, M., Moser, E. (2011). Model-free fMRI group analysis using FENICA. NeuroImage, 55(1), 185–193.

Shehzad, Z., Kelly, A.M., Reiss, P.T., Gee, D.G., Gotimer, K., Uddin, L.Q., Lee, S.H., Margulies, D.S., Roy, A.K., Biswal, B.B., Petkova, E., Castellanos, F.X., Milham, M.P. (2009). The resting brain: unconstrained yet reliable. *Cereb Cortex, 19(10),* 2209-29.

Sheline, Y. I., Raichle, M. E., Snyder, A. Z., Morris, J. C., Head, D., Wang, S., & Mintun, M. A. (2010). Amyloid plaques disrupt resting state default mode network connectivity in cognitively normal elderly. *Biol Psychiatry, 67(6),* 584-587.

Shrout, P. E. & Fleiss, J. L. (1979) Intraclass correlations: uses in assessing rater reliability. Psychol Bull *86(2):* 420-428.

Shulman, G. L., Fiez, J. A., Corbetta, M., Buckner, R. L., Miezin, F. M., et al. (1997). Common blood flow changes across visual tasks: II: decreases in cerebral cortex. *J. Cogn. Neu- rosci., 9,* 648–63.

Siegel, J. S., Power, J. D., Dubis, J. W., Vogel, A. C., Church, J. A., Schlaggar, B. L., Petersen, S. E. (2014). Statistical Improvements in Functional Magnetic Resonance Imaging Analyses Produced by Censoring High-Motion Data Points. Human Brain Mapping, *35(5),* 1981–1996.

Sladky, R., Friston, K. J., Tröstl, J., Cunnington, R., Moser, E., & Windischberger, C. (2011). Slice-timing effects and their correction in functional MRI. NeuroImage, *58,* 588–594.

Turner, R., Howseman, A., Rees, G. E., Josephs, O., & Friston, K. (1998). Functional magnetic resonance imaging of the human brain: data acquisition and analysis. Exp Brain Res, 123 *(1-2),* 5–12.

Van Dijk, K. R. A., Hedden, T., Venkataraman, A., Evans, K. C., Lazar, S. W., & Buckner, R. L. (2010). Intrinsic functional connectivity as a tool for human connectomics: theory, properties, and optimization. *J Neurophysiol, 103,* 297–321.

Van Dijk, K. R. A., Sabuncu, M. R., & Buckner, R. L. (2012). The influence of head-motion on intrinsic functional connectivity MRI. NeuroImage, 59*(1),* 431–8.

Vincent, J. L., Kahn, I., Snyder, A. Z., Raichle, M. E., Buckner, R. L. (2008). Evidence for a frontoparietal control system revealed by intrinsic functional connectivity. *J Neurophysiol*., *100*, 3328–42.

Washington, S. D., Gordon, E. M., Brar, J., Warburton, S., Sawyer, A. T., Wolfe, A., Mease-Ference, E. R., Girton, L., Hailu, A., Mbwana, J., Gaillard, W. D., Kalbfleisch, M. L., VanMeter, J. W. (2014). Dysmaturation of the default mode network in autism. *Human Brain Mapping, 35(4),* 1284-96.

Westbrook, C., Kaut Roth, C., Talbot, J. (2005). MRI in Practice, third ed. *Blackwell Publishing.*

Zeng, L. L., Wang, D., Fox, M. D., Sabuncu, M., Hu, D., Ge, M., Buckner, R. L., Liu, H. (2014). Neurobiological basis of head-motion in brain imaging. *Proc. Natl. Acad. Sci. U.S.A.,* 111, 6058–62.

Zhou, Y., Dougherty, J. H., Hubner, K. F., Bai, B., Cannon, R. L., & Hutson, R. K. (2008). Abnormal connectivity in the posterior cingulate and hippocampus in early Alzheimer's disease and mild cognitive impairment. Alzheimer's & Dementia : The Journal of the Alzheimer's Association, 4*(4)*, 265–270.

Zuo X. N., Anderson J. S., Bellec P., Birn R. M., Biswal B. B., Blautzik J., Breitner J. C., Buckner, R. L., Calhoun, V. D., Castellanos, F. X., Chen, A., Chen, B., Chen, J., Chen, X., Colcombe, S. J., Courtney, W., Craddock, R. C., Di Martino, A., Dong, H. M., Fu, X., Gong, Q., Gorgolewski, K. J., Han, Y., He, Y., He, Y., Ho, E., Holmes, A., Hou, X. H., Huckins, J., Jiang, T., Jiang, Y., Kelley, W., Kelly, C., King, M., LaConte, S. M., Lainhart, J. E., Lei, X., Li, H. J., Li, K., Li, K., Lin, Q., Liu, D., Liu, J., Liu, X., Liu, Y., Lu, G., Lu, J., Luna, B., Luo, J., Lurie, D., Mao, Y., Margulies, D. S., Mayer, A. R., Meindl, T., Meyerand, M. E., Nan, W., Nielsen, J. A., O'Connor, D., Paulsen, D., Prabhakaran, V., Qi, Z., Qiu, J., Shao, C., Shehzad, Z., Tang, W., Villringer, A., Wang, H., Wang, K., Wei, D., Wei, G. X., Weng, X. C., Wu, X., Xu, T., Yang, N., Yang, Z., Zang, Y. F., Zhang, L., Zhang, Q., Zhang, Z., Zhang, Z., Zhao, K.,

Zhen, Z., Zhou, Y., Zhu, X. T., Milham, M. P. (2014). An open science resource for establishing reliability and reproducibility in functional connectomics. *Sci. Data. 1:140049*.

Zuo, X. N., Kelly, C., Adelstein, J. S., Klein, D. F., Castellanos, F. X., & Milham, M. P. (2010). Reliable intrinsic connectivity networks: Test-retest evaluation using ICA and dual regression approach. NeuroImage, 49, 2163–2177.

Motion and tSNR measures	Interleaved		Sequential		Non-parametric
	VOMOCO	SLOMOCO	VOMOCO	SLOMOCO	Friedman test
Median displacements	0.19 ± 0.17 mm	1.1 ± 0.9 mm	0.2 ± 0.1 mm	1.2 ± 1.1 mm	χ^2 (3, n = 46) = 112.9, p < 0.001
Maxima displacements	0.8 ± 0.7 mm	2 ± 1 mm	1.2 ± 1.4 mm	2.8 ± 2.6 mm	χ^2 (3, n = 46) = 93.3, p < 0.001
Full-brain tSNR (before preprocessing)	22.2 ± 4.3	22.2 ± 4.3	22.6 ± 4.4	22.6 ± 4.4	N.A.
Gray matter tSNR (after preprocessing)	277.8 ± 62.9	349.7 ± 72.4	273.8 ± 68	317.4 ± 69.9	χ^2 (3, n = 46) = 76, p < 0.001

Table 1. Head movement statistics after head motion correction. The table shows averaged median and maxima volume-to-volume head movement displacements across individuals for each slice-order acqusition protocol and head movement correction method. Second to last and bottom lines report the tSNR prior any head-motion correction and after data preprocessing, respectively. Head movement displacement timeseries were derived from the straight sum of the absolute value of 6 head movement parameters of 194 time points in length. Head movement estimates and the tSNR are similar across slice-order protocols but differ across head-motion correction methods.

	Intrinsic DMN connectivity				
	VOMOCO		SLOMOCO		
Region of interest	Interleaved	Sequential	Interleaved	Sequential	Non-parametric Friedman test
DMN	7.3 ± 0.9	6.6 ± 0.7	6.5 ± 0.8	7.0 ± 1.0	$\chi^2(3, n = 46) = 26.18, p < 0.001$
PCC	7.4 ± 1.1	7.2 ± 0.9	7.1 ± 1.2	8.0 ± 1.4	$\chi^2(3, n = 46) = 9.36, p = 0.025$
ACC	7.0 ± 1.0	5.6 ± 0.5	5.6 ± 0.5	6.1 ± 0.7	$\chi^2(3, n = 46) = 56.03, p < 0.001$
LPC	7.6 ± 1.1	7.0 ± 0.9	6.5 ± 1.0	7.2 ± 1.2	$\chi^2(3, n = 46) = 23.7, p < 0.001$

Table 2. Functional Connectivity results. Average (SD) mean z-scores across participants and sessions under each slice acquisition and motion correction method (columns) for each ROI (rows). The last column provides non-parametric analysis of variance output (uncorrected). Significant statistical effects were found across conditions in each single ROI ($p < 0.05$). Except for PCC (slice order effects only), for all other areas the effects were significant for both slice order and motion correction method. See text for more information.

Region of interest	Reproducibility measure	VOMOCO		SLOMOCO		Statistics (Friedman test)
		Interleaved	Sequential	Interleaved	Sequential	
DMN	% Error	(7.2 ± 4.8)%	(5.5 ± 4.1)%	(6.3 ± 5.2)%	(7.8 ± 5)%	$\chi^2(3, n = 23) = 2.5, p = 0.5$
	ICC *(C.I.)*	0.45 *(0.29 - 0.55)*	0.51 *(0.35 - 0.61)*	0.40 *(0.24 – 0.51)*	0.50 *(0.37 – 0.61)*	N.A.
PCC	% Error	(7.3 ± 5)%	(6.2 ± 5)%	(8.1 ± 6.9)%	(10.3 ± 6.1)%	$\chi^2(3, n = 23) = 5.8, p = 0.1$
	ICC *(C.I.)*	0.33 *(0.19 – 0.40)*	0.40 *(0.23 – 0.51)*	0.43 *(0.26 – 0.53)*	0.52 *(0.37 – 0.63)*	N.A.
ACC	% Error	(8.2 ± 5.2)%	(4.3 ± 4.2)%	(5.7 ± 4.4)%	(7 ± 4.5)%	$\chi^2(3, n = 23) = 56.0, p = 0.06$
	ICC *(C.I.)*	0.50 *(0.36 – 0.60)*	0.45 *(0.29 – 0.55)*	0.59 *(0.27 – 0.73)*	0.47 *(0.36 – 0.58)*	N.A.
LPC	% Error	(8 ± 5.4)%	(6.9 ± 5.5)%	(7.4 ± 5.6)%	(8.7 ± 5.6)%	$\chi^2(3, n = 23) = 3.7, p = 0.3$
	ICC *(C.I.)*	0.49 *(0.36 – 0.60)*	0.56 *(0.26 – 0.68)*	0.36 *(0.20 – 0.46)*	0.47 *(0.28 – 0.57)*	N.A.

Connectivity Method	Reproducibility Measure	VOMOCO		SLOMOCO		Statistics (Friedman test)
		Interleaved	Sequential	Interleaved	Sequential	
ROI-Based Analysis 10 mm radius sphere	Absolute Percent Error	(27 ± 16.3)%	(28.5 ± 20)%	(30.8 ± 23.5)%	(27.6 ± 19.4)%	χ^2 (3, n = 23) = 0.34, p = 0.9
ICA-Based Analysis	Absolute Percent Error	(7.2 ± 4.8)%	(5.5 ± 4.1)%	(6.3 ± 5.2)%	(7.8 ± 5)%	χ^2 (3, n = 23) = 2.5, p = 0.5
Statistics (Paired Samples t-test)		t(22) = -7.45; p < 0.001	t(22) = -8.65; p < 0.001	t(22) = -3.98; p = 0.001	t(22) = -8.7; p < 0.001	

Supplementary Table 1. Comparison of ROI-based and ICA-based analyses for the DMN: effects of motion-correction and slice-order acquisition methods on TRT reproducibility. Intrinsic DMN reproducibility results for the ROI-based (top row) and the ICA-based analysis (middle row). The TRT reliability from both approaches is not influenced by slice-order acquisition and motion correction methods (last column). Moreover, the TRT reliability of the ROI-based approach registers significantly larger test-retest percent errors than the ICA-based approach in all conditions examined (bottom row).

Table 3. Test-retest reproducibility of the DMN (z-scores > 2.3): slice-order acquisition and head motion correction effects. The table shows the average (SD) TRT reproducibility errors across participants and relative ICCs (C.I.) for each condition of interest (columns) and ROI (rows). The last column reports statistical evaluations using non-parametric Friedman test. No significant statistical differences were found in TRT reproducibility errors across conditions in any ROI (DMN: default mode network; PCC: posterior cingulate cortex; ACC: anterior cingulate and medial prefrontal cortex; LPC: left/right latero-parietal cortex).

Region of interest	Jaccard Index				Statistics (Friedman test)
	VOMOCO		SLOMOCO		
	Interleaved	Sequential	Interleaved	Sequential	
DMN	(43 ± 7)%	(36 ± 13)%	(40 ± 6)%	(41 ± 6)%	$\chi^2(3, n = 23) = 6.8, p = 0.08$
PCC	(49 ± 10)%	(44 ± 30)%	(53 ± 8)%	(64 ± 8)%	$\chi^2(3, n = 23) = 29.8, p < 0.001$
ACC	(35 ± 8)%	(29 ± 28)%	(37 ± 7)%	(21 ± 7)%	$\chi^2(3, n = 23) = 31.5, p < 0.001$
LPC	(52 ± 10)%	(39 ± 20)%	(32 ± 9)%	(40 ± 9)%	$\chi^2(3, n = 23) = 20.6, p < 0.001$

Table 4.

Test-retest reproducibility of spatial DMN overlap. Average (SD) Jaccard index across participants is reported for each slice-order acquisition and motion correction method (columns) and ROI (rows). Non-parametric pairwise Friedman's tests testing effects among columns are reported in the last column (uncorrected). Even though no significant statistical effects were found when considering the entire DMN, slice-order protocol and/or motion correction method effects were found in each single DMN node, suggesting higher intra-network susceptibility to these factors. DMN: default mode network; PCC: precuneus and posterior cingulate cortex; ACC: anterior cingulate and medial prefrontal cortex; LPL: left/right parietal cortex.

Reproducibility of the Intrinsic Default Mode Network: Influence of fMRI Slice-Order Acquisition and Head-Motion Correction Methods (doi: 10.1089/brain.2016.0450)
This manuscript has been peer-reviewed and accepted for publication, but has yet to undergo copyediting and proof correction. The final published version may differ from this proof.

Brain Connectivity

Test-Retest Reproducibility of the Intrinsic Default Mode Network: Influence of fMRI Slice-Order Acquisition and Head-Motion Correction Methods (doi: 10.1089/brain.2016.0450)
This paper has been peer-reviewed and accepted for publication, but has yet to undergo copyediting and proof correction. The final published version may differ from this proof.